Remarkable low-temperature hydrogen cycling kinetics of Mg enabled by VH_x nanoparticles

Xuelian Zhang[a,†], Xin Zhang[a,†], Lingchao Zhang[a], Zhenguo Huang[b], Fang Fang[c]*, Yaxiong Yang[d], Mingxia Gao[a], Hongge Pan[a,d], Yongfeng Liu[a,d]*

[a]State Key Laboratory of Silicon Materials and School of Materials Science and Engineering, Zhejiang University, Hangzhou 310027, China.

[b]School of Civil & Environmental Engineering, University of Technology Sydney, 81 Broadway, Ultimo, NSW, 2007, Australia.

[c]Department of Materials Science, Fudan University, Shanghai, 200433 China.

[d]Institute of Science and Technology for New Energy, Xi'an Technological University, Xi'an, 710021, China.

[†]These authors contributed equally to this work.

*Corresponding author:

Email: mselyf@zju.edu.cn (Y.F.L.); f_fang@fudan.edu.cn (F.F.)

Abstract:

Nanoscaled catalysts have attracted much more attention due to their more abundant active sites and better dispersion than their bulky counterparts. In this work, VH_x nanoparticles smaller than 10 nm in average size are successfully synthesized by a simple solid-state ball milling coupled with THF washing process, which are proved to be highly effective in enhancing the hydrogen absorption/desorption kinetics of MgH_2 at moderate temperatures. The nano-VH_x modified MgH_2 releases hydrogen from 182 °C, which is 88 °C lower than that of additive-free MgH_2. The release of hydrogen amounts to 6.3 wt% H within 10 min at 230 °C and 5.6 wt% H after 30 min at 215 °C with initial vacuum. More importantly, the dehydrogenated MgH_2+10 wt% nano-VH_x rapidly absorbs 5.2 wt% H within 3 min at 50 °C under 50 bar H_2. It even takes up 4.3 wt% H within 30 min at room temperature (25 °C) under 10 bar H_2, exhibiting superior hydrogenation kinetics to most of the previous reports. Mechanistic analyses disclose the

reversible transformation between V and V-H species during the hydrogen desorption-absorption process. The homogeneously distributed V-based species is believed to act as hydrogen pump and nucleation sites for MgH_2 and Mg, respectively, thus triggering fast hydrogenation/dehydrogenation kinetics.

Keywords: hydrogen storage, MgH_2, catalysts, VH_x nanoparticles, hydrogenation kinetics

1. Introduction

The development and application of hydrogen energy has attracted increasing attentions since hydrogen possesses a high energy density of 142 MJ kg^{-1} and the final product is free of pollution [1]. However, the widespread utilization of hydrogen energy, especially for on-board applications, still faces many challenges. The most important is the storage and transportation of hydrogen with a safe, efficient and economic technique [2]. With high hydrogen densities and moderate operating pressures, solid-state hydrogen storage is a preferable option in the future [3]. Magnesium hydride, MgH_2, with 7.6 wt% of hydrogen capacity and excellent reversibility, has been widely studied for mobile hydrogen storage applications. However, high operating temperatures (>350 °C) are required to achieve reasonable rates of hydrogen cycling by MgH_2 because of its stable thermodynamics and sluggish kinetics [4,5]. Over the past few decades, various strategies have been developed to improve the hydrogen cycling performance, including alloying Mg with other metals, catalyst modification and fabricating nanostructures [6-9].

Catalyst is of critical importance in improving the kinetics of hydrogen storage in metal hydrides [10,11]. It is generally accepted that the hydrogenation rate of a metal is related to three main factors, including (i) the dissociation of H_2 molecules at the surface, (ii) the penetration of H atoms from the surface into the metal, and (iii) the diffusion of H atoms through the hydride layer into the bulk metal. A very high energy is required for H_2 dissociation on the

surface of bulk Mg particles due to the lack of d-electron [12]. In this respect, transition metals, especially Ni, Ti and Nb, and their compounds have been extensively studied for the improvement of hydrogen sorption by Mg because they can enable fast and effective dissociation of H_2 molecules [8,13-25]. For instance, Holtz and Imam reported a 50% increase in hydrogen capacity and a decrease in the onset hydrogenation temperature from 275 to 175 °C, while adding 1 mol% Ni into Mg [15]. The onset dehydrogenation temperature of MgH_2 was reduced to 143 °C by introducing 4 mol% porous Ni nanofibers [16]. The 5 mol% Ti-catalyzed Mg nanopowders absorbed 5.2 wt% H at 150 °C under 10.3 MPa H_2 and the release of hydrogen started from ~190 °C, which was lowered by 191 °C than the onset temperature of pristine MgH_2 [17]. With $TiCl_3$ as a precursor, Cui *et al.* created a multi-valence Ti catalyzed MgH_2, which enabled the release of 5 wt% H within 15 min at 250 °C [18]. The 5 wt% Ti_3C_2-modified MgH_2 released 6.2 wt% H within 1 min at 300 °C and absorbed 6.1 wt% H within 30 s at 150 °C [19]. Shao *et al*. observed 40 times increase in the hydrogenation rate for the nanocrystalline Ti-catalyzed MgH_2 at 300 °C [20]. By doping 5 wt% TiO_2 nanosheet into MgH_2, hydrogen desorption amounted to 6.0 wt% within 3.2 min at 260 °C [21]. The addition of 0.2 mol% Nb_2O_5 enabled 6.9 wt% H release from MgH_2 in 140 s at 300 °C [22]. The catalytic activity of Nb_2O_5 was further enhanced by N doping [23]. The hydrogen release of MgH_2-10 wt% N-Nb_2O_5 was observed from 170 °C, 130 °C lower than that of pristine MgH_2, and the dehydrogenated sample was fully hydrogenated below 100 °C under 50 bar H_2. Through the addition of 7 wt% $TiNb_2O_7$, Mg started absorbing hydrogen even at room temperature and rapidly took up 4.5 wt% H within 3 min at 150 °C [24]. Much higher catalytic activity was attained by fabricating 2D nanoflake shaped bimetallic Ti–Nb oxide [25].

Vanadium works well as a catalyst for the dissociation of H_2 molecules. It is worth highlighting that V-containing MgH_2 showed the fastest desorption kinetics compared with those modified with Ti, Mn, Fe and Ni, as illustrated by Liang *et al* [26]. Similar observation was also reported by Vincent *et al* [27]. In comparison with V and VC, a much faster absorption

kinetics was measured for the VCl_3-catalyzed MgH_2 because the dehydrogenated MgH_2-5 wt% VCl_3 composite absorbed 6.0 wt% H after 7.5 min at 350 °C [28]. The hydrogenation performance was further improved by fabricating carbon nanobox-supported V_2O_3 nanoparticles [29]. For the 9 wt% nano-V_2O_3@C-catalyzed sample, full hydrogenation was achieved within 700 s at 150 °C under 50 bar H_2.

Unfortunately, transition metal oxides and halides usually react with MgH_2/Mg due to the favorable thermodynamics, which consumes the active species for storing hydrogen. As a result, transition metal hydrides are believed to be much better to balance catalytic activity and practical hydrogen capacity. For example, TiH_2, YH_2, NbH and ScH_2 have been evaluated for their catalytic properties [30-34]. In particular, the addition of TiH_2 contributed to a significant improvement in the kinetics of dehydrogenation and hydrogenation compared with commercial MgH_2 [30,31]. The dehydrogenation of the milled MgH_2−0.1TiH_2 started at about 180 °C, much lower than that of the milled undoped MgH_2 (280 °C). More specifically, the dehydrogenated sample absorbed 4 wt% H in 4 h even at room temperature. However, no attempt has been reported to improve hydrogen storage properties of MgH_2 by directly adding nanoscaled VH_x.

Herein, VH_x nanoparticles (nano-VH_x) were successfully synthesized via a simple solid-state ball milling coupled with THF washing process. The resultant VH_x nanoparticles were measured to be smaller than 20 nm in size and significantly improved the hydrogen sorption kinetics of Mg at lower temperatures. The MgH_2+7 wt% nano-VH_x composite started releasing hydrogen from 182 °C and hydrogen desorption amounted to 6.8 wt% H while heating to 275 °C at 2 ºC min^{-1} of ramping rate. Isothermal measurements indicate that the 7 wt% nano-VH_x -modified MgH_2 desorbed ~6.3 wt% H within 10 min at 230 °C and absorbed ~4.9 wt% H in 30 min at 50 °C. Increasing the addition of nano-VH_x resulted in much faster hydrogen absorption kinetics. The fully desorbed 10 wt% nano-VH_x-modified sample rapidly took up 5.2 wt% H in only 3 min at 50 °C, indicating >10 times increase in the average hydrogenation rate. Such fast

hydrogenation kinetics at moderate conditions have been rarely reported before. The underlying catalytic mechanism of VH_x nanoparticle was investigated and discussed.

2. Experimental section

2.1 Synthesis of nano-VH_x

Commercial vanadium trichloride (VCl_3, Aladdin, 99.9%), lithium hydride (LiH, Alfa Aesar, 97%) and tetrahydrofuran (THF, Sinopharm Chemical Reagent Co., 99.5%) were purchased and used without purification for the preparation of nanoscaled VH_x. VH_x nanoparticles (nano-VH_x) were synthesized by try ball milling VCl_3 and LiH (Eq. 1) followed by washing with THF:

$$3\mathrm{LiH}+\mathrm{VCl_3} \rightarrow \mathrm{VH}_x + 3\mathrm{LiCl} + \frac{3-x}{2}\mathrm{H_2} \qquad (1)$$

THF was dried over calcium hydride (CaH_2, Alfa Aesar, 95%) to remove water prior to use. Mechanochemical reaction between VCl_3 and LiH with a mole ratio of 1:3 were conducted on a planetary ball mill (QM-3SP4, Nanjing) at 400 rpm for 4 h. The as-milled black powders were collected and washed with anhydrous THF to remove the by-product LiCl under Ar protection. After centrifugation, the precipitation was dried under dynamic vacuum at ambient temperature for 1 h to produce the final VH_x nanoparticles.

2.2 Preparation of catalyzed MgH_2 system

MgH_2 was synthesized in our own laboratory. Commercial Mg powders (Macklin, 20-340 mesh, 95%) were first hydrogenated at 340 °C for 12 h under 20 bar H_2. The hydrogenated powders were then milled and further treated at 380 °C for 12 h under 50 bar H_2. Finally, the catalyzed MgH_2 systems were prepared by mixing MgH_2 with nano-VH_x at given weight ratios. Mechanical mixing was conducted on a planetary ball mill at 500 rpm for 3 h. The milling jar was charged with 10 bar H_2 and the ball-to-sample weight ratio was set at 120:1. All the sample handling was carried out in an Etelux Lab2000 glove box filled with high-purity Ar.

2.3 Characterization methods

X-ray diffraction (XRD) characterizations were carried out on a Rigaku MiniFlex 600 (Japan) with Cu K_α radiation operated at 40 kV and 15 mA with a scanning rate of 5° min^{-1}. A custom-designed sample holder covered with Scotch tape was used to prevent exposure of samples to air and moisture during the tests. Scanning electron microscope (SEM, Hitachi SU8010) and transmission electron microscope (TEM, FEI Tecnai G2 F20 S-TWIN) were employed to observe morphologies and analyze microstructures. Elemental distribution was characterized by energy dispersive X-ray spectrometer (EDS, X-Max) attached to the SEM and TEM facilities. X-ray photoelectron spectroscopy (XPS) measurements were performed using a Thermo Scientific ESCALAB 250Xi with a monochromatic Al Kα X-ray source (1486.6 eV) under a base pressure of ~8.8×10^{-10} mbar. The adventitious C peak at 284.8 eV was used as the reference to calibrate XPS data.

A home-built temperature-programmed desorption (TPD) system equipped with a mass spectrometer (MS, Hiden QIC-20) was used to characterize dehydrogenation behavior. Approximately 15 mg of sample was loaded into a stainless-steel tube reactor and heated from ambient temperature to desired temperatures at a preset heating rate with Ar as a carrier gas. The quantitative measurements of hydrogen desorption and absorption were conducted on a homemade Sievert's type apparatus. For non-isothermal tests, the sample was heated with a heating rate of 2 °C min^{-1} under vacuum. The dehydrogenated sample was rehydrogenated from room temperature to 250 °C at 1 °C min^{-1} with an initial hydrogen pressure of 50 bar. For isothermal experiments, the sample was first quickly (10 °C min^{-1} of heating rate) heated to the desired temperatures and then maintained for a certain duration at this temperature.

3. Results and discussion

3.1 Synthesis and Characterization of nano-VH_x

The nano-VH_x was synthesized by a simple solid-state mechanochemical reaction between VCl_3 and LiH following by a THF washing process, as schematically illustrated in Fig. 1. VCl_3

and LiH were first loaded into a stainless-steel jar inside the glovebox and then ball milled. Ball milling induced the occurrence of chemical reaction between VCl_3 and LiH (Eq. 1) as evidenced by the H_2 signal (Fig. S1) and the formation of LiCl (Fig. 2a). The by-product LiCl was removed after washing with THF as evidenced by the disappearance of its characteristic XRD diffraction peaks. Only several broad diffraction peaks indexed to cubic structure (a ~ 4.02 Å) were detected in the XRD profile, possibly related to V-based species (Fig. 2a). EDS point analyses indicated the existence of V (Fig. 2b), which was further confirmed by EDS mapping (Fig. S2). A liberation of H_2 was observed while heating from room temperature to 450 °C (Fig. 2c). We therefore believe that the resultant sample is mainly composed of V and H, denoted as VH_x based upon Eq. (1). Here, the value of x in the as-synthesized VH_x was determined to be ~1.17 by volume release measurement associated with XRD analyses (Fig. 2d). Further SEM observation displays irregular nanoparticles with aggregation to some degree (Fig. 2e). The size distribution based on TEM image (Fig. 2f) is ~7.1 nm of average size for VH_x nanoparticles.

3.2 Catalytic effects of nano-VH_x on dehydrogenation of MgH_2

The synthesized VH_x nanoparticles (referred as nano-VH_x) were mechanically milled with MgH_2 to evaluate its effectiveness on catalyzing dehydrogenation and rehydrogenation. The designed weight concentrations are y = 0, 1, 3, 5, 7 and 10 in MgH_2+y wt% nano-VH_x. Mechanical milling treatment of 3 h enabled homogeneous dispersion of nano-VH_x in MgH_2 matrix as demonstrated by the EDS mapping results (Fig. 3a). In contrast, segregation was observed in the composite (Fig. 3b) where bulk VH_x, obtained by hydriding commercial metallic V, measuring in micron size (Fig. S3) was ball milled with MgH_2 using the identical parameters. This indicates an excellent dispersibility of nano-VH_x due to the largely reduced particle size, which provides much better contact and more active sites for catalyzing the dissociation of Mg-H and H-H bonds, as discussed later.

Fig. 4a shows the qualitative dehydrogenation behavior measured by means of TPD-MS. The as-milled pristine MgH_2 started dehydrogenation from 275 °C and peaked at 327 °C with

one shoulder peak at 358 °C. The small shoulder peak at higher temperatures is mainly attributed to a small amount of distinctly large particles of the as-milled MgH_2 (Fig. S4). After adding 1 wt% nano-VH_x, two obvious dehydrogenation peaks were detected at 250 °C and 279 °C, both lower than those of pristine sample. The distinct peak splitting is possibly due to the insufficient catalysis. Increasing the addition of nano-VH_x to 7 wt%, only one dehydrogenation peak was observed in the TPD-MS curve and the peak temperature was reduced to 230 °C, representing 97 °C lower than that of pristine MgH_2. When the content of nano-VH_x reached 10 wt%, no additional reduction was attained for the dehydrogenation temperature. It is therefore believed that the addition of 7 wt% nano-VH_x is sufficient for catalyzing dehydrogenation of MgH_2 in the present study.

Quantitative volumetric release was further measured and compared. As shown in Fig. 4b, the hydrogen desorption of as-milled pristine MgH_2 occurred at a temperature range of 275-380 °C with ~7.4 wt% of total capacity, which agrees well with the TPD-MS results. The presence of nano-VH_x induces a remarkable low-temperature shift in the volumetric release curve. The onset dehydrogenation temperature was drastically decreased to 220 °C and then further moved to 182 °C when the loading of nano-VH_x increased from 1 wt% to 7 wt%. Correspondingly, the finishing temperature of dehydrogenation process was lowered to 300 °C and the practical hydrogen capacity was reduced to 6.8 wt%. For the 10 wt% nano-VH_x-containing sample, the volumetric release curve is nearly the same except a reduction in hydrogen capacity. Thus, 7 wt% nano-VH_x is the optimal loading which enables dehydrogenation from 182 °C and 6.8 wt% H at 300 °C.

Isothermal dehydrogenation measurements indicate the remarkably improved kinetics for nano-VH_x-modified MgH_2 at lowered temperatures. As shown in Fig. 4c, the MgH_2+7 wt% nano-VH_x sample rapidly liberated ~6.3 wt% H within 10 min at 230 °C and ~5.6 wt% H within 30 min at 215 °C. As a contrast, nearly no hydrogen was released from the as-milled pristine MgH_2 even at a higher temperature of 250 °C within 30 min. More importantly, the MgH_2+7

wt% nano-VH_x sample could desorb 3.4 wt% and 1.5 wt% H within 30 min when dwelling at 200 °C and 185 °C, respectively, demonstrating remarkably improved low-temperature dehydrogenation performance. The dehydrogenation kinetics of MgH_2+7 wt% nano-VH_x is superior to other V compounds-catalyzed MgH_2 systems, as displayed in Fig. 4d [29,35-40]. When operating at 300 °C and 0.15 bar of back pressure, nearly 6.8 wt% H was released within only 3 min (Fig. S5a), remarkably higher than that of the well-known MgH_2-V system which liberated less than 5.5 wt% H under similar conditions [41]. Even with 1.0 bar back pressure, the 7 wt% nano-VH_x-containing sample also liberated 6.5 wt% H in the first 10 min, which is comparable with V catalyst-modified MgH_2 samples operating under vacuum (Fig. S5b and Table S1).

The advantage of nanocatalysts was further evidenced when compared with the bulk VH_x, which was synthesized by hydriding commercial V powders (Beijing Xing Rong Yuan, purity 99%) at 500 °C under 50 bar H_2. As shown in Fig. S6a, the dehydrogenation temperatures of MgH_2 milled with bulk VH_x for 3 h are obviously higher than those of the nano-VH_x-containing sample. Specifically, the middle-point temperature corresponding to the half of hydrogen desorption was measured to be 282 °C, which is 53 °C higher than that of nano-VH_x-modified sample. This can be attributed to the inhomogeneous distribution and poor contact of bulk VH_x with MgH_2 caused by the larger particle size (Fig. 3b). Moreover, the catalytic activity of nano-VH_x also outperforms reported V-based catalysts, including V, VN and VCl_3, considering that the dehydrogenation temperatures of the nano-VH_x-modified MgH_2 are lowest among these materials (Fig. S6b) and only 3 h ball milling was required in this work in contrast to 24 h reported in the literature.

3.3 Catalytic effects of nano-VH_x on rehydrogenation

The fully dehydrided MgH_2+7 wt% nano-VH_x sample was rehydrogenated under 50 bar H_2 in both isothermal and non-isothermal modes to evaluate the effect of nano-VH_x on the hydrogen absorption performance. Fig. 5a illustrates the non-isothermal hydrogenation curves of

dehydrided MgH_2 and nano-VH_x-modified MgH_2. Interestingly, these two samples displayed very different hydrogen uptake behaviors, indicating various hydrogenation kinetics. Hydrogen uptake by the dehydrided pristine MgH_2 can be divided into three regions, including a sluggish increase in hydrogen amount between 106 and 160 °C, a rapid increase between 160 and 220 °C, and a slow increase to saturation between 220 and 260 °C. This is mainly originated from the poor catalytic activity of metallic Mg for the dissociation of H-H bonds due to the lack of d-electron, consequently resulting in the high on-set temperature for hydrogenation. In contrast, only two regions were observed for the 7 wt% nano-VH_x-modified sample because hydrogen uptake rapidly increased below 50 °C and then slowly increased until 250 °C. The total hydrogen uptake amounted to 6.3 wt%. Here, the onset temperature of hydrogenation was ~80 °C lower than that of pristine sample. This hydrogenation performance is also largely superior to the bulk VH_x-modified samples and other V-based catalyst-containing samples (Fig. S6c and d). This finding indicates that nano-VH_x facilitates the dissociation of H-H bonds and the formation of Mg-H bonds, therefore effectively enhancing the hydrogenation kinetics and lowering the hydrogenation temperatures even to room temperature (25 °C). In addition, it should be mentioned that relatively stable hydrogen cycling was obtained for the nano-VH_x-modified sample. As shown in Fig. S7, the reversible hydrogen capacity stabilized at ~6 wt% after 10 cycles.

Hydrogen uptake kinetics was further investigated by isothermal experiments. The results are shown in Fig. 5b. It is observed that ~5.8 wt% of H was absorbed by the dehydrogenated 7 wt% nano-VH_x-containing MgH_2 within 1 min at 150 °C under 50 bar H_2. When hydriding at 100 °C, it rapidly took up 5 wt% H in 1 min. More importantly, the 7 wt% nano-VH_x-modified sample absorbed ~4.9 wt% and 3.5 wt% H within 30 min when dwelled at 50 °C and 25 °C, respectively, indicating remarkably enhanced low-temperature hydrogenation kinetics. Much faster hydrogenation kinetics was obtained while increasing the loading of nano-VH_x to 10 wt% (Fig. 5c). At 50 °C, the fully dehydrogenated MgH_2+10 wt% nano-VH_x sample absorbed 5.3

wt% H in 3 min. The average rate of hydrogenation is ~10 times higher than that of 7 wt% nano-VH_x-containing sample (the inset of Fig. 5c). Even operating at 25 °C, the hydrogen capacity reached 4.9 wt% in 30 min. The measured hydrogenation kinetics of nano-VH_x-containing MgH_2 at such low temperatures outperform most catalyzed MgH_2 systems reported previously (Fig. 5d and Table S2). Although the reaction rate slowed down to some extent at 10 bar H_2, hydrogen uptake still amounted to 5.2 wt% and 4.4 wt% by the 10 wt% nano-VH_x-containing sample within 30 min at 50 and 25 °C (Fig. S8), respectively. In particular, the nano-VH_x-containing sample absorbed 4.3 wt% H within 10 min at 50 °C, nearly twice that of the reported MgH_2-V system [41].

3.4 The catalyst role played by nano-VH_x

To understand the role played by nano-VH_x, the enthalpy change and apparent activation energy for hydrogen storage reaction were measured. Fig. 6a shows the pressure-composition isothermal (PCI) desorption curves of MgH_2+7 wt% nano-VH_x sample at 200, 225, 250, and 275 °C. All curves display one distinct pressure plateau at a given temperature, indicating that the addition of nano-VH_x did not alter the dehydrogenation pathway of MgH_2. Hydrogen in MgH_2+7 wt% nano-VH_x sample was completely liberated at 200 °C in the PCI mode, which gave rise to the formation of metallic Mg as characterized by XRD (Fig. S9). This result also demonstrates remarkably improved dehydrogenation kinetics of nano-VH_x modified MgH_2 at lowered temperatures. By fitting with the van't Hoff equation (Fig. 6b), the desorption enthalpy change was calculated to be ~74.0 kJ mol^{-1} H_2 for MgH_2+7 wt% nano-VH_x sample, very close to the value of pristine MgH_2 (~76 kJ mol^{-1} H_2) [4,5]. We therefore believe that the addition of nano-VH_x has not changed the hydrogen storage thermodynamics of MgH_2. Here, it should be noted that in contrast to isothermal hydrogenation kinetic measurement, where the amount of hydrogen absorbed by the sample is different at different temperatures, the same amount of hydrogen is absorbed at different temperatures in the PCI curves. For PCI measurements, the

input hydrogen pressure was gradually increased from zero at a given temperature, and the duration was long enough to reach equilibrium at every given hydrogen pressure. Hydrogenation is therefore sufficient. In hydrogenation kinetic experiments, however, a given high hydrogen pressure was directly applied on the sample, which may cause insufficient hydrogenation.

Fig. 6c presents the TPD-MS curves of pristine MgH_2 and nano-VH_x-containing MgH_2 with various heating rates. The nano-VH_x-modified sample presents a remarkable low-temperature shift in the dehydrogenation process. The apparent activation energy for dehydrogenation was calculated by fitting Kissinger's plot (Fig. 6d), which is approximately 89.0 kJ mol^{-1} for MgH_2+7 wt% nano-VH_x, a ~37% reduction in comparison with pristine MgH_2 (140.5 kJ mol^{-1}). The largely lowered activation energy barrier reveals the catalytic role played by nano-VH_x. As such, the remarkably low desorption temperature was attributed to the largely reduced kinetic energy barrier for hydrogen storage in the nano-VH_x-containing sample. For the hydrogenation process, the activation energy was determined to be ~23.3 kJ mol^{-1} by fitting the isothermal curves with Johnson–Mehl–Avrami (JMA) equation, as shown in Fig. S10. This value is comparable to that of the traditional interstitial metal hydride of $LaNi_5$ (~20 kJ mol^{-1}) [42], well interpreting the room-temperature hydrogenation capability of the nano-VH_x-modified Mg system. Moreover, the Avrami exponent *n* determined from the slopes of JMA plots are 0.73-0.82, ranging from 0.5 to 1, which indicates a site saturation model for the nucleation and growth of MgH_2 based on previous reports [7,43,44].

To understand the V-based catalytic species, the dehydrogenated/hydrogenated samples at different stages were collected and characterized by XRD and XPS. High-resolution XPS spectra of V exhibited only zero-valent V (V^0) at 519.9 and 512.3 eV for the as-prepared nano-VH_x (Fig. S11a), and no obvious change in the XPS spectra was observed after ball milling VH_x with MgH_2 and even dehydrogenation/hydrogenation (Fig. S11b), possibly due to the solid solution structure of V-based hydrides as widely reported [45]. Moreover, it should be

mentioned that V-related peaks were not detected in the XRD profile of 7 wt% nano-VH_x-containing MgH_2 (Fig. S12). As a result, to detect V-based species, the loading of nano-VH_x was increased to 20 wt%. Note that MgH_2 with 7 wt% and 20 wt% VH_x loading display nearly identical dehydrogenation performance (Fig. S13). As shown in Fig. 7a, a gradual transformation from MgH_2 to Mg was identified when heating the MgH_2+20 wt% nano-VH_x sample, indicating that the released hydrogen mainly originates from the decomposition of MgH_2. Simultaneously, a careful observation at 2θ = 38-44° revealed a conversion of VH_x species to metallic V (Fig. 7b). After ball milling MgH_2 with nano-VH_x, a low-angle shoulder peak was observed at 38-40°, which is attributed to the VH_x species because it is invisible in pristine MgH_2 (Fig. S14). Upon heating, this peak gradually moved to high angle and an XRD peak associated with metallic V was observed at 300 °C. Comparing the TPD curves of nano-VH_x and MgH_2, as shown in Fig. 2c and Fig. 4a, the dehydrogenation of nano-VH_x was prior to MgH_2. The partially dehydrogenated VH_x phase facilitates attracting H from the adjacent MgH_2 phase because the strong electronic interaction between V and H. This consequently weakens the Mg-H bonding of MgH_2 in the phase boundary between VH_x and MgH_2, and makes the nucleation of Mg in the phase boundary much easier than that in the MgH_2 phase. In addition, the partial liberation of H gave rise to the formation of H vacancy, which works as hydrogen diffusion pathway and accelerates the migration of H. As reported previously, the diffusion of H atoms is much easier in the MgH_2-V systems than in the pure MgH_2 [46]. We therefore believe that the presence of nano-VH_x improved the dehydrogenation kinetics of MgH_2 by promoting diffusion of H and accelerating nucleation rates of Mg.

The dehydrogenated MgH_2+20 wt% nano-VH_x sample was also rehydrogenated under 50 bar H_2 in a dynamic heating mode. As shown in Fig. 7c, the diffraction peaks of MgH_2 became dominant in the XRD profile along with the gradual disappearance of metallic Mg when heating the dehydrogenated sample to 30 °C. This indicates an ultrafast hydrogen absorption by the 20 wt% VH_x-containing sample at room temperature (Fig. S15). Correspondingly, the diffraction

peaks of metallic V disappeared with the emergence of a new broad peak at ~42° in spite of very weak intensity after hydrogenation, representing the reformation of VH_x species. Further hydrogenation at 150 °C induced a slight increase in the intensity of VH_x without other apparent changes. Hydrogen absorption by Mg generally includes the adsorption and dissociation of molecular hydrogen at the surface, the penetration and diffusion of atomic hydrogen into Mg matrix, and the formation of Mg-H bond. It is well known that pristine metallic Mg exhibits very low reactivity towards H_2 because of the lack of d-orbital electrons, and metallic V with 3d electron largely facilitates the adsorption and dissociation of H_2. Thus, the metallic V in the dehydrogenated nano-VH_x-containing MgH_2 composite acts as active sites to adsorb and dissociate H_2 molecules. When the H concentration in V-H reaches certain extent, the dissociated H atoms are then transferred to the Mg-V interfaces which facilitates the nucleation of MgH_2. In other words, the VH_x plays the roles of hydrogen pump and nucleation sites of MgH_2. As a result, high catalytic effect and abundant nucleation sites originated from nano-VH_x in MgH_2 enable ultrafast hydrogen absorption even at room temperature.

The important catalytic role played by nano-VH_x was further evidenced by TEM observations and EDS mapping analyses. Here, the sample powders were directly dispersed on Cu grids inside a glovebox, and the excess powders were blown off with an aurilave. The TEM sample was then transferred to TEM chamber using air-tight holder. The HRTEM images were analyzed through the Gatan Digital Micrograph software to obtain the corresponding fringes. As shown in Fig. 8a-d, the nano-VH_x dispersed homogeneously into MgH_2 matrix after 3 h ball milling, a distinctly shorter duration compared with other V-based catalysts [26,28,29]. The homogeneous dispersion of nano-VH_x remained upon dehydrogenation (Fig. 8e-g), and the diffraction fringes of metallic V were visible from the HRTEM image of fully dehydrogenated sample (Fig. 8h), in consistent with the XRD result as discussed above. Upon dehydrogenation and hydrogenation to a certain degree, coexistence of MgH_2 and metallic Mg crystals was observed (Fig. 9). It should be noted that MgH_2 crystals surrounded by VH_x readily transform

into metallic Mg while there is still MgH_2 when direct contact with VH_x is absent (Fig. 9a), and vice versa (Fig. 9b). This observation indicates the catalytic role of nano-VH_x in improving hydrogen storage properties of MgH_2.

4. Conclusion

In this work, VH_x nanoparticles with average size of ~7.1 nm were successfully synthesized by ball milling the mixture of VCl_3 and LiH followed by THF washing to remove by-product. The resultant VH_x nanoparticles displayed superior catalytic activity for hydrogen storage in MgH_2. With the addition of 7 wt% nano-VH_x into MgH_2, the onset dehydrogenation temperature was remarkably reduced by 88 °C from 270 to 182 °C. The practical dehydrogenation capacity was determined to be 6.8 wt% when heating to 300 °C. The fully dehydrogenated sample absorbed ~5.8 wt% of H within 1 min at 150 °C under 50 bar H_2. When operating at 50 °C, hydrogen uptake amounted to ~4.9 wt% in 30 min, exhibiting superior low-temperature hydrogenation kinetics. More importantly, increasing the loading of nano-VH_x to 10 wt% induced 10 times enhancement in the hydrogenation rate at 50 °C. Analyses of thermodynamics and kinetics revealed a negligible desorption enthalpy change but a largely reduced kinetic energy barrier. The activation energy for hydrogen desorption was reduced by ~37% from 140.5 kJ mol^{-1} to 89.0 kJ mol^{-1} with a loading of 7 wt% nano-VH_x. It is therefore believed that the nano-VH_x plays a catalyst role. Structural characterization indicated a reversible transformation between VH_x and V upon dehydrogenation and hydrogenation. The largely reduced particle size enables the homogeneous dispersion of VH_x, which worked as hydrogen pumps and nucleation sites, consequently facilitating the low-temperature dehydrogenation and hydrogenation. This finding provides new insights on catalytic mechanism of transition metal hydride-based catalysts.

Notes

The authors declare no competing financial interest.

Data availability

All data included in this study are available upon request from the corresponding author.

Acknowledgements

We gratefully acknowledge the financial support received from the National Outstanding Youth Foundation of China (52125104), the Natural Science Foundation of Zhejiang Province (LD21E010002), the National Natural Science Foundation of China (52001277), the Fundamental Research Funds for the Central Universities (2021FZZX001-09), and the National Youth Top-Notch Talent Support Program.

Appendix A. Supplementary data

Supplementary data associated with this article can be found in the online version at doi:

References

[1] I.P. Jain, Int. J. Hydrogen Energy 34 (2009) 7368–7378.

[2] T. He, P. Pachfule, H. Wu, Q. Xu, P. Chen, Nat. Rev. Mater. 1 (2016) 16067.

[3] J. Zheng, C.-G. Wang, H. Zhou, E. Ye, J.W. Xu, Z.B. Li, X.J. Loh, Research 1 (2021) 3750689.

[4] Q. Li, Y.F. Lu, Q. Luo, X.H. Yang, Y. Yang, J. Tan, Z.H. Dong, J. Dang, J.B. Li, Y. Chen, B. Jiang, S.H. Sun, F.S. Pan, J. Magnes. Alloy. 9 (2021) 1922–1941.

[5] V.A. Yartys, M.V. Lototskyy, E. Akiba, R. Albert, V.E. Antonov, J.R. Ares, M. Baricco, N. Bourgeois, C.E. Buckley, J.M. Bellosta von Colbe, J.-C. Crivello, F. Cuevas, R.V. Denys, M. Dornheim, M. Felderhoff, D.M. Grant, B.C. Hauback, T.D. Humphries, I. Jacob, T.R. Jensen, P.E. de Jongh, J.-M. Joubert, M.A. Kuzovnikov, M. Latroche, M. Paskevicius, L. Pasquini, L. Popilevsky, V.M. Skripnyuk, E. Rabkin, M.V. Sofianos, A. Stuart, G. Walker, H. Wang, C.J. Webb, M. Zhu, Int. J. Hydrogen Energy 44 (2019) 7809–7859.

[6] M. Zhu, Y.S. Lu, L.Z. Ouyang, H. Wang, Materials 6 (2013) 4654–4674.

[7] Q. Luo, Y.L. Guo, B. Liu, Y.J. Feng, J.Y. Zhang, Q. Li, K.C. Chou, J. Mater. Sci. Technol. 44 (2020) 171–190.

[8] X.L. Zhang, Y.F. Liu, X. Zhang, J.J. Hu, M.X. Gao, H.G. Pan, Mater. Today Nano 9 (2020) 100064.

[9] Q. Luo, J.D. Li, B. Li, B. Liu, H.Y. Shao, Q. Li, J. Magnes. Alloy. 7 (2019) 58–71.

[10] B. Sakintuna, F. Lamari-Darkrimb, M. Hirscherc, Int. J. Hydrogen Energy 32 (2007) 1121–1140.

[11] A.W.C. van den Berg, C.O. Areán, Chem. Commun. (2008) 668–681.

[12] I.P. Jain, C. Lal, A. Jain, Int. J. Hydrogen Energy 35 (2010) 5133–5144.

[13] Q.H. Hou, X.L. Yang, J.Q. Zhang, ChemistrySelect 6 (2021) 1589–1606.

[14] J.G. Zhang, Y.F. Zhu, L.L. Yao, C. Xu, Y.N. Liu, L.Q. Li, J. Alloys Compd. 782 (2019) 796–823.

[15] R. L. Holtz, M.A. Imam, J. Mater. Sci. 34 (1999) 2655–2663.

[16] J. Chen, G.L. Xia, Z.P. Guo, Z.G. Huang, H.K. Liu, X.B. Yu, J. Mater. Chem. A 3 (2015) 15843–15848.

[17] Y.J. Choi, J.W. Choi, H.Y. Sohn, T. Ryu, K.S. Hwang, Z.Z. Fang, Int. J. Hydrogen Energy 34 (2009) 7700–7706.

[18] J. Cui, H. Wang, J.W. Liu, L.Z. Ouyang, Q.G. Zhang, D.L. Sun, X.D. Yao, M. Zhu, J. Mater. Chem. A 1 (2013) 5603–5611.

[19] Y.F. Liu, H.F. Du, X. Zhang, Y.X. Yang, M.X. Gao, H.G. Pan, Chem. Commun. 52 (2016) 705–708.

[20] H. Shao, M. Felderhoff, F. Schüth, C. Weidenthaler, Nanotechnology 22 (2011) 235401.

[21] M. Zhang, X.Z. Xiao, X.W. Wang, M. Chen, Y.H. Lu, M.J. Liu, L.X. Chen, Nanoscale 11 (2019) 7465–7473.

[22] G. Barkhordarian, T. Klassen, R. Bormann, Scr. Mater. 49 (2003) 213–217.

[23] K. Wang, X. Zhang, Z.H. Ren, X.L. Zhang, J.J. Hu, M.X. Gao, H.G. Pan, Y.F. Liu, Energy Storage Mater. 23 (2019) 79–87.

[24] L.C. Zhang, K. Wang, Y.F. Liu, X. Zhang, J.J. Hu, M.X. Gao, H.G. Pan, Nano Research 14 (2021) 148–156.

[25] K.C. Xian, M.H. Wu, M.X. Gao, S. Wang, Z.L. Li, P.Y. Gao, Z.H. Yao, Y.F. Liu, W.P. Sun, H.G. Pan, Small, 2022 2107013.

[26] G. Liang , J. Huot, S. Boily, A. Van Neste, R. Schulz, J. Alloys Compd. 292 (1999) 247–252.

[27] S.D. Vincent, J. Lang, J. Huot, J. Alloys Compd. 512 (2012) 290–295.

[28] M.O.T. da Conceição, M.C. Brum, D.S. dos Santos, J. Alloys Compd. 586 (2014) S101–S104.

[29] Z.Y. Wang, Z.H. Ren, N. Jian, M.X. Gao, J.J. Hu, F. Du, H.G. Pan, Y.F. Liu, J. Mater. Chem. A 6 (2018) 16177–16185.

[30] J. Lu, Y.J. Choi, Z.Z. Fang, H.Y. Sohn, E. Rönnebro, J. Am. Chem. Soc. 131 (2009) 15843–15852.

[31] M. Lotoskyy, R. Denys, V.A. Yartys, J. Eriksen, J. Goh, S.N. Nyamsi, C. Sita, F. Cummings, J. Mater. Chem. A 6 (2018) 10740–10754.

[32] A.R. Yavari, J.F.R. de Castro, G. Vaughan, G. Heunen, J. Alloys Compd. 353 (2003) 246–251.

[33] X.L. Luo, D.M. Grant, G.S. Walker, J. Alloys Compd. 622 (2015) 842–850.

[34] Q. Li, Y. Li, B. Liu, X.G. Lu, T.F. Zhang, Q.F. Gu, J. Mater. Chem. A 5 (2017) 17532–17543.

[35] Z.Y. Lu, H.J. Yu, X. Lu, M.C. Song, F.Y. Wu, J.G. Zheng, Z.F. Yuan, L.T. Zhang, Rare Met. 40 (2021) 3195–3204.

[36] Y.P. Pang, Y.F. Wang, J.H. Yang, S.Y. Zheng, Compos. Commun. 26 (2021) 100781.

[37] H.Z. Liu, C.L. Lu, X.C. Wang, L. Xu, X.T. Huang, X.H. Wang, H. Ning, Z.Q. Lan, J. Guo, ACS Appl. Mater. Interfaces 13 (2021) 13235−13247.

[38] X. Zhang, Z.Y. Shen, N. Jian, J.J. Hu, F. Du, J.H. Yao, M.X. Gao, Y.F. Liu, H.G. Pan, Int. J. Hydrogen Energy 43 (2018) 3327–23335.

[39] J.H. Zang, S.F. Wang, R.R. Hu, H. Man, J.C. Zhang, F. Wang, D.L. Sun, Y. Song, F. Fang, J. Mater. Chem. A 9 (2021) 8341–8349.

[40] J.H. Zang, S.F. Wang, F. Wang, Z.Y. Long, F.J. Mo, Y.H. Xia, F. Fang, Y. Song, D.L. Sun, J. Mater. Chem. A 8 (2020) 14935–14943.

[41] G. Liang, J. Huot, S. Boily, A. Van Neste, R. Schulz, J. Alloys Compd. 291 (1999) 295–299.

[42] Q. Li, X. Lin, Q. Luo, Y.A. Chen, J.F. Wang, B. Jiang, F.S. Pan, Int. J. Miner. Metall. Mater. 29 (2022) 32–48.

[43] Y.P. Pang, D.K. Sun, Q.F. Gu, K.-C. Chou, X.L. Wang, Q. Li, Cryst. Growth Des. 16 (2016) 2404–2415.

[44] Y.F. Liu, K. Luo, Y.F. Zhou, M.X. Gao, H.G. Pan, J. Alloys Compd. 481 (2009) 472–479.

[45] A.Y. Esayed, D.O. Northwood, Int. J. Hydrogen Energy 17 (1992) 41–52.

[46] D.W. Zhou, J.S. Liu, B. Ping, Sci. China Ser. E-Tech. Sci. 51 (2008) 979–988.

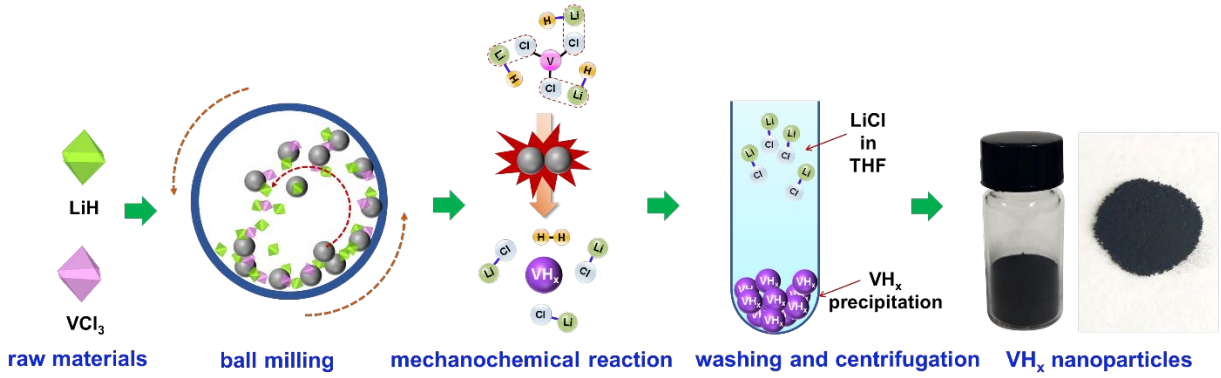

Fig. 1. Schematic illustration of the preparation of nano-VH_x.

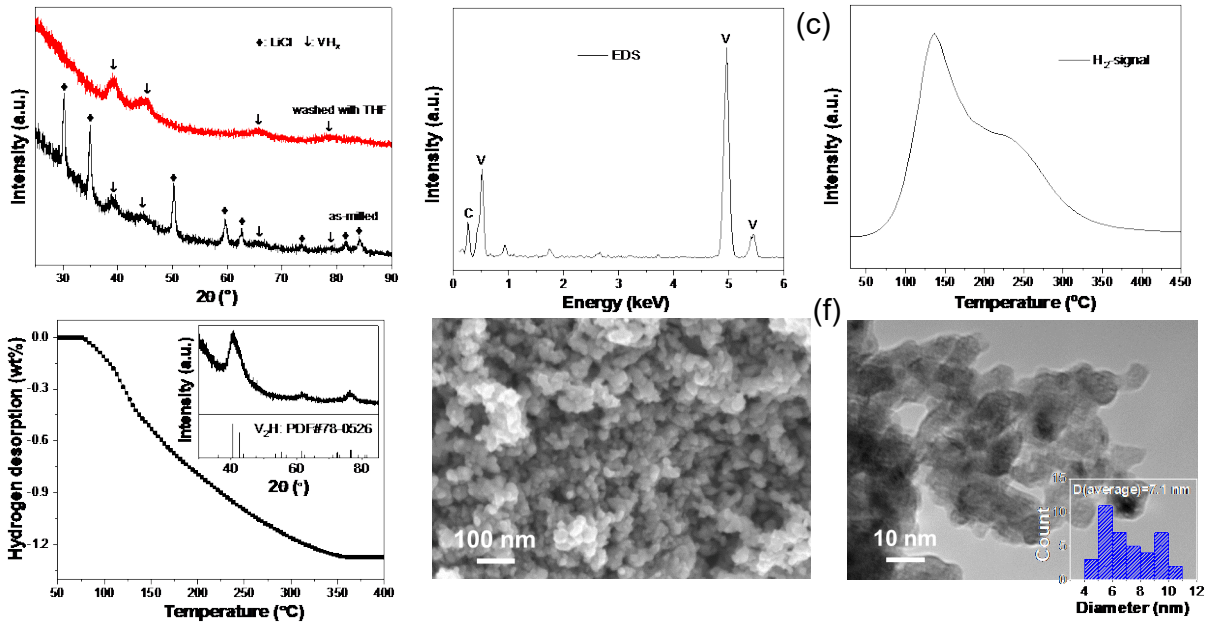

Fig. 2. (a) XRD patterns of the mixture (VCl_3+LiH) after ball milling (black) and washing with THF (red), (b) EDS pattern, (c) TPD-MS signal, (d) volumetric hydrogen release curve, (e) SEM and (f) TEM images of the as-obtained product (Inset: particle size distribution).

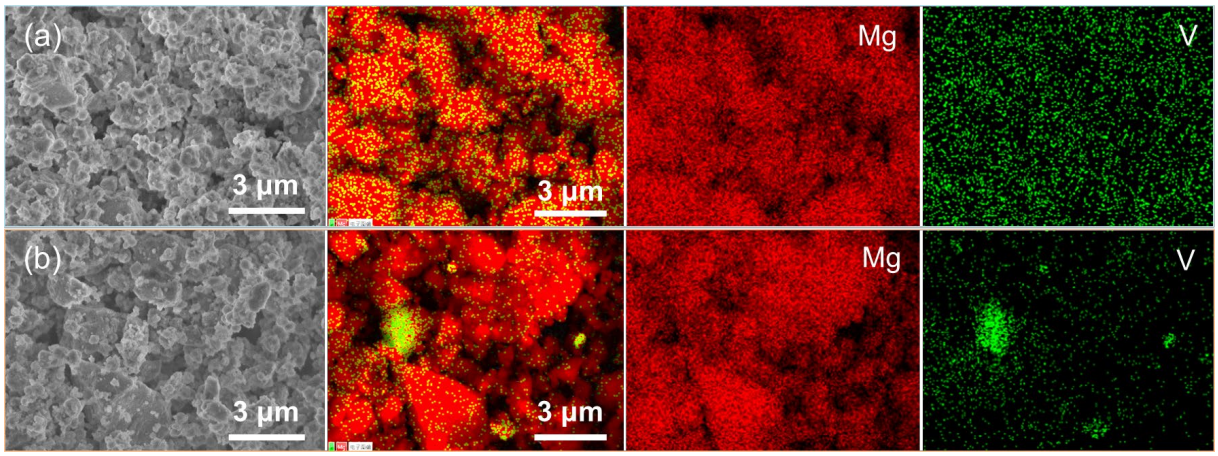

Fig. 3. EDS mapping of Mg and V for MgH_2 milled with (a) nano-VH_x and (b) bulk VH_x.

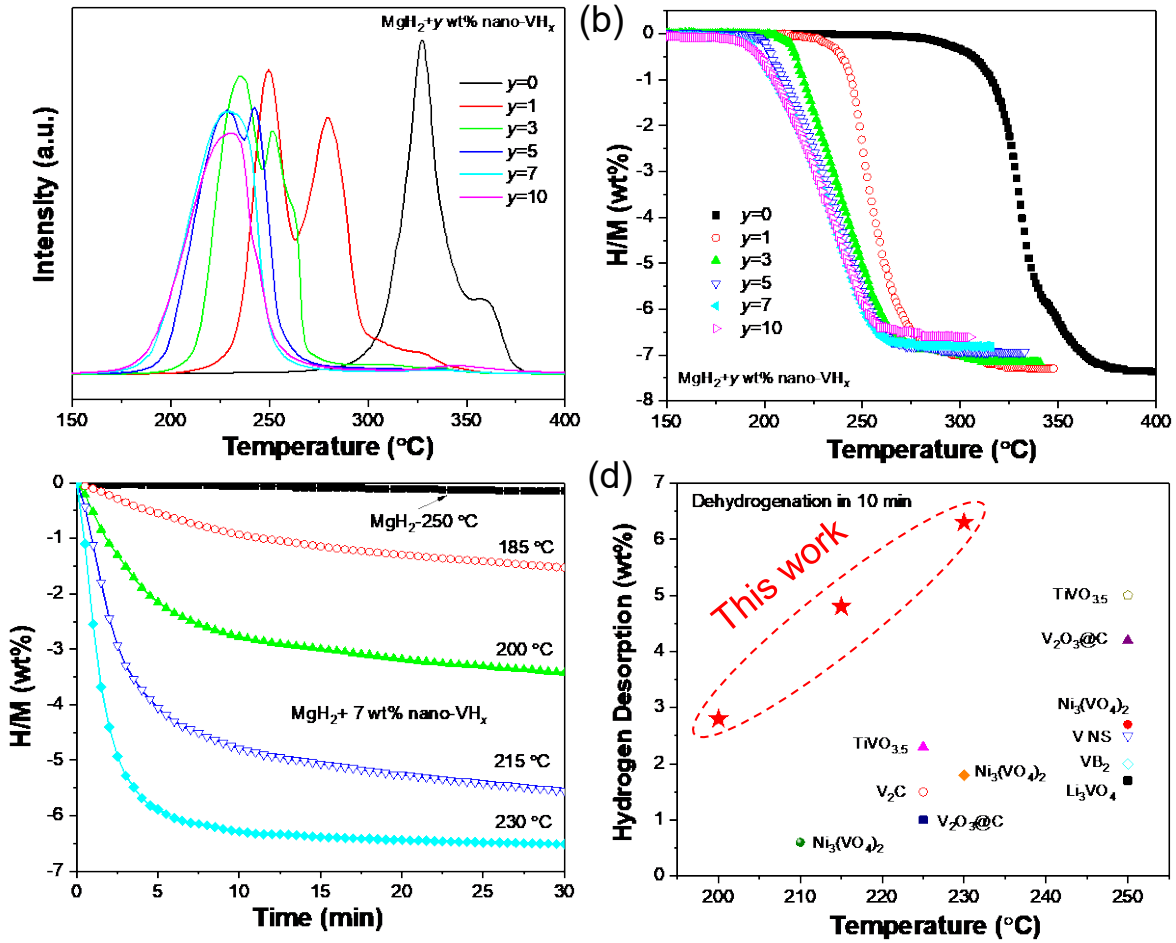

Fig. 4. (a) TPD and (b) volumetric hydrogen release curves of MgH_2+y wt% nano-VH_x (y = 0, 1, 3, 5, 7, 10) samples. (c) Isothermal hydrogen desorption curves of pristine MgH_2 and nano-VH_x-containing MgH_2 at various temperatures. (d) Comparison of hydrogen desorption capacity in the first 10 min of nano-VH_x-containing MgH_2 with reported catalyst-modified samples at various temperatures.

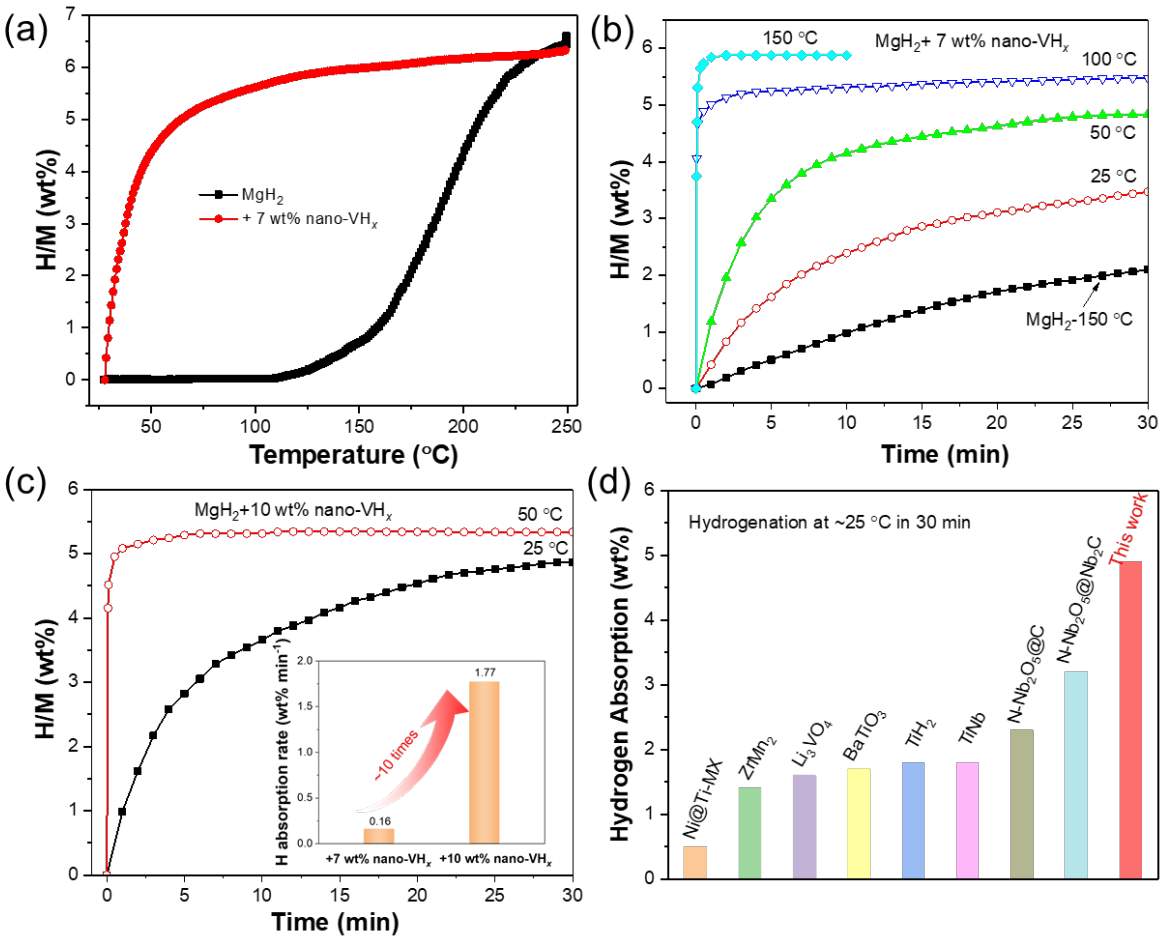

Fig. 5. (a) Non-isothermal and (b,c) isothermal hydrogen absorption curves of dehydrogenated pristine MgH_2 and nano-VH_x-containing MgH_2 under 50 bar H_2. The inset shown in (c) is the average hydrogen absorption rates of dehydrogenated MgH_2 doped with 7 wt% nano-VH_x and 10 wt% nano-VH_x. (d) Comparison of hydrogen absorption capacity in the first 30 min of dehydrogenated 10 wt% nano-VH_x-containing MgH_2 with reported catalyst-modified samples at room temperature.

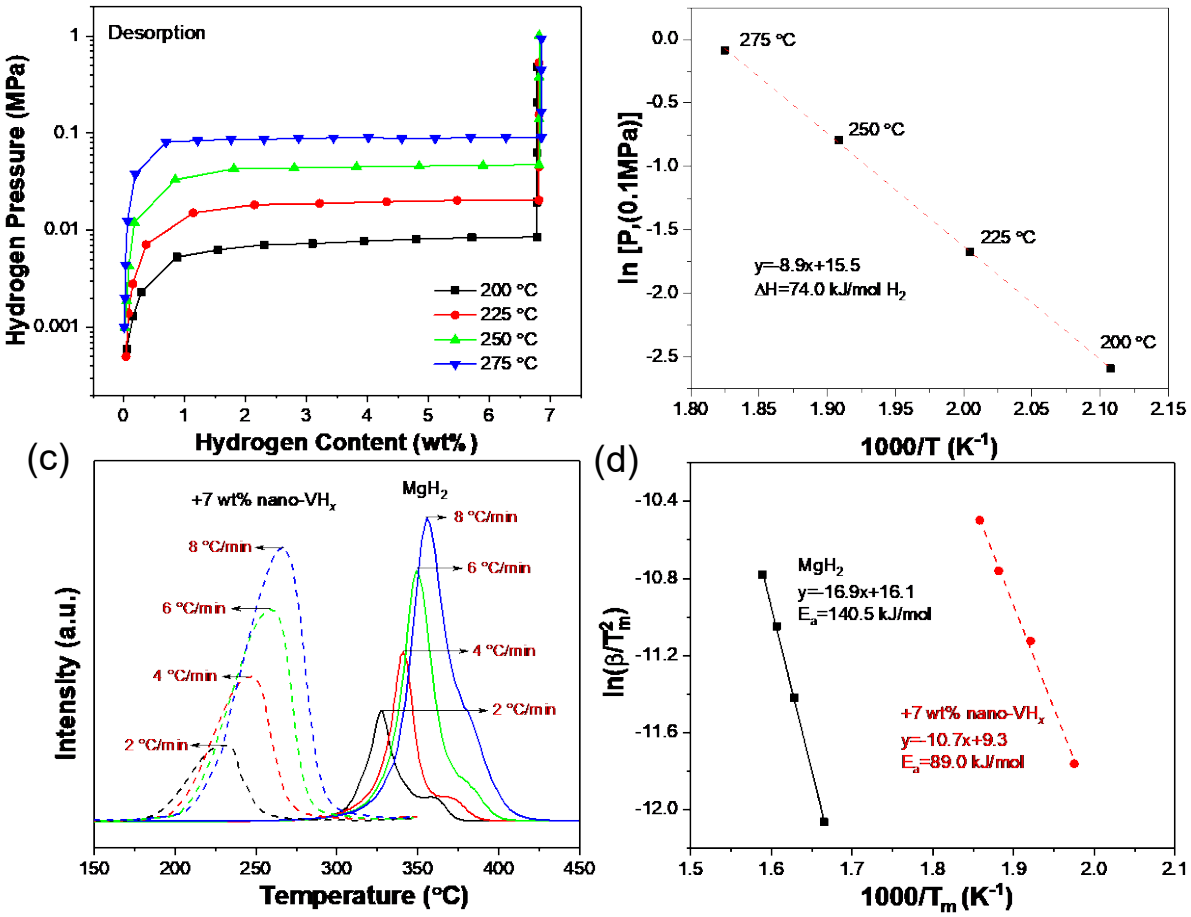

Fig. 6. (a) PCI curves and (b) van't Hoff plots for the MgH_2+7 wt% nano-VH_x sample. (c) TPD curves with various heating rates and (d) Kissinger's plots of pristine MgH_2 and nano-VH_x-containing MgH_2.

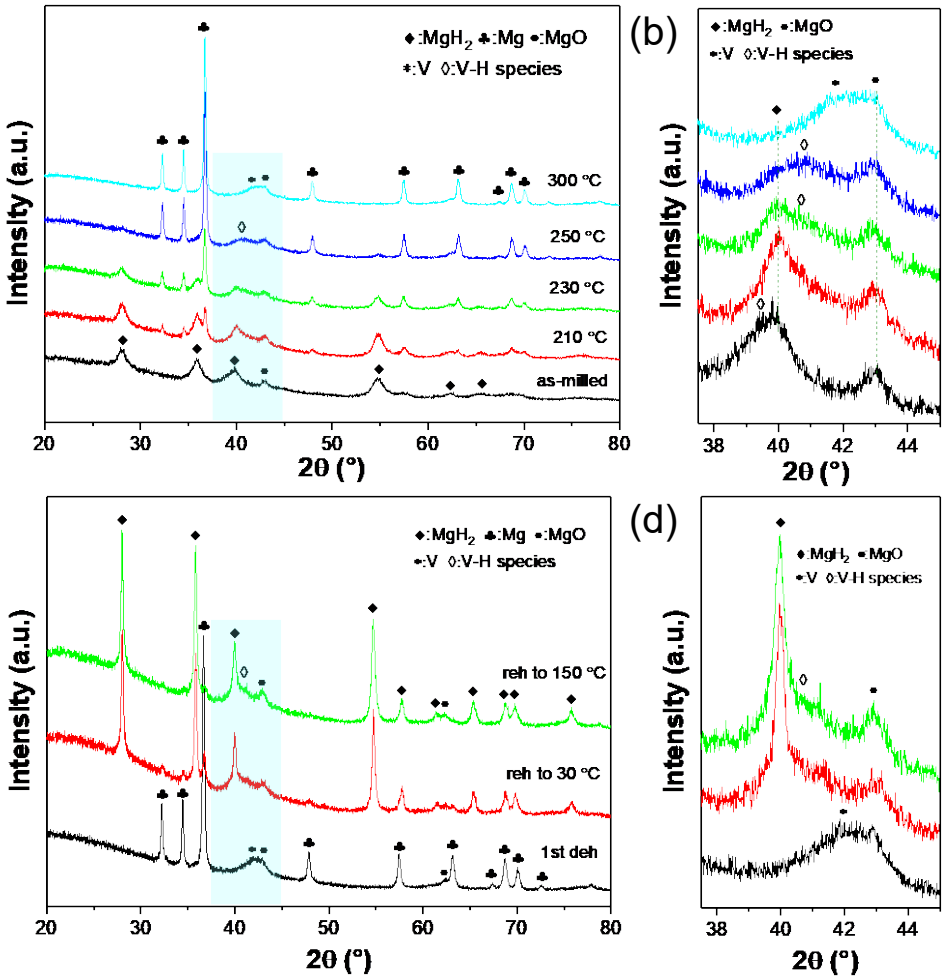

Fig. 7. (a) XRD patterns and (b) the enlarged patterns in the range of 37.5-45° of the MgH_2+20 wt% nano-VH_x sample dehydrogenated at different stages. (c) XRD patterns and (d) the enlarged pattern in the range of 37.5-45° of the dehydrogenated MgH_2+20 wt% nano-VH_x sample hydrogenated at different stages.

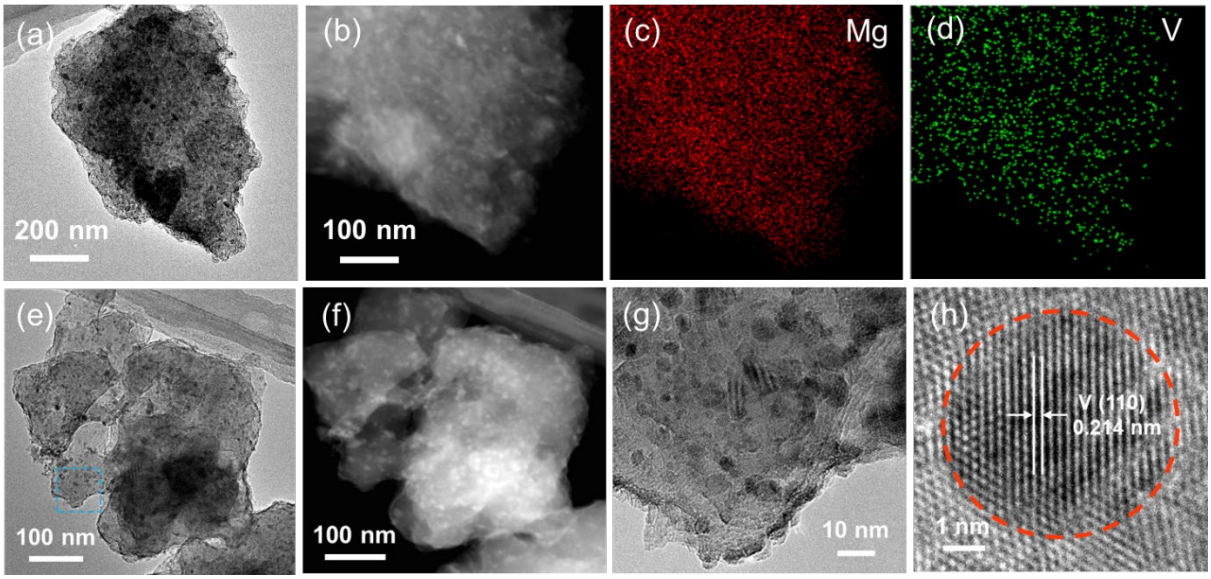

Fig. 8. (a,b) TEM image and (c,d) the corresponding EDS mappings of the as-prepared 7 wt% nano-VH_x-containing MgH_2. (e-g) TEM and (h) HRTEM images of 7 wt% nano-VH_x-containing sample after full dehydrogenation.

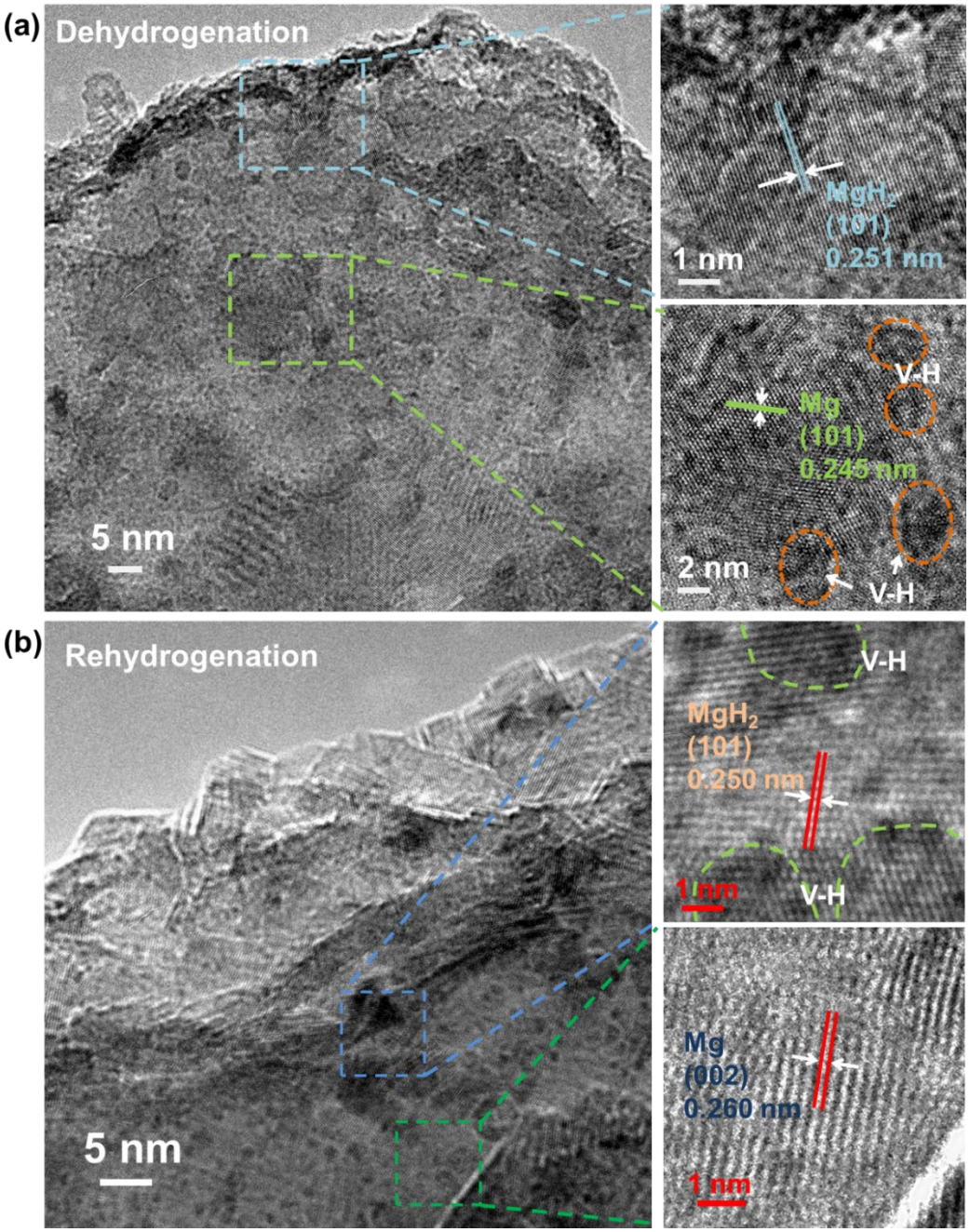

Fig. 9. HRTEM images of the nano-VH_x-containing MgH_2 (a) after releasing 1.5 wt% H and (b) after retaking up 1.5 wt% H.